

On the improvement of alveolar-like microfluidic devices for efficient blood oxygenation

M. Malankowska^{a,b,c}, *I. Pellejero*^d, *I. Julian*^{a,b}, *H.S. Rho*^c, *P. Pinczowski*^e,
R.M. Tiggelaar^{c,f}, *H. Gardeniers*^c, *R. Mallada*^{a,b,g}, *M.P. Pina*^{a,b,g,*}

^aInstituto de Nanociencia y Materiales de Aragón (INMA), Universidad de Zaragoza-CSIC, 50009 Zaragoza, Spain.

^bDepartamento de Ingeniería Química y Tecnología del Medio Ambiente, Universidad de Zaragoza, 50009, Spain.

^cMesoscale Chemical Systems, MESA+ Institute, University of Twente, P.O. Box 217, 11 7500 AE Enschede, The Netherlands.

^dInstitute for Advanced Materials, Public University of Navarra, Edif. Jerónimo de Ayanz, Campus Arrosadia, s/n, 31006 Pamplona-Iruña, Spain

^eVeterinary School of Zaragoza, C/ Miguel Servet 177, 50013 Zaragoza, Spain

^fMESA+ NanoLab cleanroom, MESA+ Institute, University of Twente, P.O. Box 217, 11 7500 AE Enschede, The Netherlands.

^gNetworking Research Centre on Bioengineering, Biomaterials and Nanomedicine, CIBER-BBN, 28029 Madrid, Spain

*mapina@unizar.es

This is the peer reviewed version of the following article: Malankowska, M., Pellejero, I., Julian, I., Rho, H. S., Pinczowski, P., Tiggelaar, R. M., Gardeniers, H., Mallada, R., Pina, M. P., On the Improvement of Alveolar-Like Microfluidic Devices for Efficient Blood Oxygenation. *Adv. Mater. Technol.* 2021, 6, 2001027, which has been published in final form at <https://doi.org/10.1002/admt.202001027>. This article may be used for non-commercial purposes in accordance with Wiley Terms and Conditions for Use of Self-Archived Versions.

Abstract

In this work, we study alveolar-like microfluidic devices with a horizontal membrane arrangement that demonstrate a great potential as small-scale blood oxygenator. The design criteria for the fabricated devices were to maximize the oxygen saturation level and minimize liquid chamber volume while ensuring the physiological blood flow in order to avoid thrombus formation and channel blockage during operation. The liquid chamber architecture was iteratively modified upon analysis of the fluid dynamics by computer modelling. Accordingly, two alveolar type architectures were fabricated, Alveolar Design 1 (AD1) and Alveolar Design 2 (AD2), and evaluated for oxygenation of sheep blood. The attained O₂ transfer rate at 1 mL/min of blood flow rate for both devices was rather similar: 123 mL·min⁻¹·m⁻² and 127 mL·min⁻¹·m⁻² for AD1 and AD2 microfluidic devices, respectively. Among the studied, AD2 type geometry would lead to the lowest pressure drop and shear stress value upon implementation in a scaled microfluidic artificial lung (μAL) to satisfy oxygenation requirements of a 2.0 kg neonate.

Keywords: neonates, priming volume, membrane type microfluidic contactor, optimization by computer modelling, simplified alveolar design

1. Introduction

Respiratory disorders are the leading cause of early neonatal mortality (0–7 days of age) and are the most frequent cause of admission to the special care nursery for both term (37-42 gestation weeks) and preterm infants (less than 37 weeks). Most causes of respiratory disorders result from an inability or delayed ability of a neonate's lungs to adapt to their new environment and to sufficiently oxygenate blood. Mechanical ventilation, conventionally used to compensate for the pulmonary insufficiency, may injure the lungs of premature infants (alveolar structural

damage, pulmonary oedema, inflammation, and fibrosis) or exacerbate their pre-existing conditions. Despite the progress in neonatal care following the introduction of new therapies and ventilator strategies, Extracorporeal Membrane Oxygenator (ECMO) remains life-saving support for about 600–800 neonates each year worldwide.^[1] ECMO systems support the respiratory function of a patient's natural lung, i.e. blood is withdrawn from the body and oxygenated extracorporeally before returning to the systemic circulation.^[2, 3] Oxygen is carried in blood in two forms: dissolved in plasma and reversibly bounded to haemoglobin (Hb). Haemoglobin is the oxygen-binding protein, which enables the red blood cells to transport more oxygen. Hb is remarkably efficient in carrying oxygen. It is able to use as much as 90% of its oxygen-carrying capacity due to its structure.^[4, 5] According to the Extracorporeal Life Support Organization (ELSO), over the last three decades circa 36.000 newborns across the world needed an ECMO procedure for respiratory failure, cardiac problems or extracorporeal cardiopulmonary resuscitation; and the overall survival rate is 83, 64, and 66%, respectively.^[6]

The oxygenator is the core component of the ECMO circuit. It functions as an artificial lung removing carbon dioxide and oxygenating blood. Most of the currently available oxygenators are made of microporous polypropylene or polymethylpentene hollow fibre bundles inside the hard-shelled jacket.^[2, 3] Typical values of volume in commercial ECMO circuits for neonates range from 30 up to 90 mL,^[7-9] but further efforts on simplification and miniaturization are still required to reduce the amount of blood which is withdrawn from the preterm infant body (total blood volume is about 100 mL/kg). In general, minimizing the amount of blood which is directly exposed to an artificial surface at a given time will lead to an increase of haematocrit values, advance patient recovery and reduction of post-operative blood transfusions.^[10] Furthermore, current applications for extracorporeal membrane oxygenation require full-body anticoagulation, which is not feasible for the preterm infant due to the risk for intraventricular haemorrhage.^[11] Moreover, it has to be taken into account that a valuable artificial lung technology should satisfy the requirements for human application: $1.9 \text{ mL} \cdot \text{kg}^{-1} \cdot \text{min}^{-1}$ of O_2 (to

increase the oxygen saturation in blood from 70% to 100%) with the extracorporeal bypass volume of $30 \text{ mL} \cdot \text{kg}^{-1} \cdot \text{min}^{-1}$ of blood.^[12]

According to ELSO registry reports, the rate of complication of clot formation resulting in the ECMO circuit replacement is about 20%. Despite the use of biocompatible equipment, the interaction between blood and the exogenous surface of the extracorporeal device activates both the coagulation cascade and the host inflammatory response through reactive oxygen species (ROS) production.^[13] During ECMO support, the risk of bleeding, infection and thrombotic complications is significant. The “heparin resistance”, which is a reduced ability of heparin to inhibit thrombin formation, is a specific concern for patients on ECMO since antithrombin activity is commonly decreased. Furthermore, neonates have low antithrombin levels which contribute even more to the development of heparin resistance. That is why decreasing blood-surface contact area is of paramount importance for preterm infants. As it is indicated by Chlebowski et al. the future of anticoagulation is not in providing higher doses of, for example heparin (that can cause bleeding), but an antithrombin replacement is a current standard practice.^[14] Moreover, current ELSO guidelines recommend an initial heparin infusion rate of 7.5-20.0 units/kg/h.^[15] In summary, additional technological efforts to: i) simplify ECMO circuit lines; ii) improve ECMO circuit miniaturization and biocompatibility are still required in order to reduce haemolysis and oxidative stress.

A biomimetic microfluidic technology, that is used for the creation of so called microfluidic artificial lungs (μ ALs), represents a unique opportunity for decreasing priming volume and blood contacting area, which is especially relevant in the case of neonates. In addition, it presents some exceptional advantages over ECMO devices: i) controlled dimensions and shape of vascular channels, ii) physiologic blood flow that is achieved by mimicking the natural lung structure and properties and iii) easier access for cellularization which leads to improved biocompatibility of the material.^[10-12, 16-20] Microfluidic artificial lung is an innovative approach, where blood flows through branched vascular microchannels, while pure oxygen (or

air) is introduced on the other side of the device and diffuses from the gas side across the permeable membrane into the blood. A conceptual drawing of such device is shown below (Figure 1).

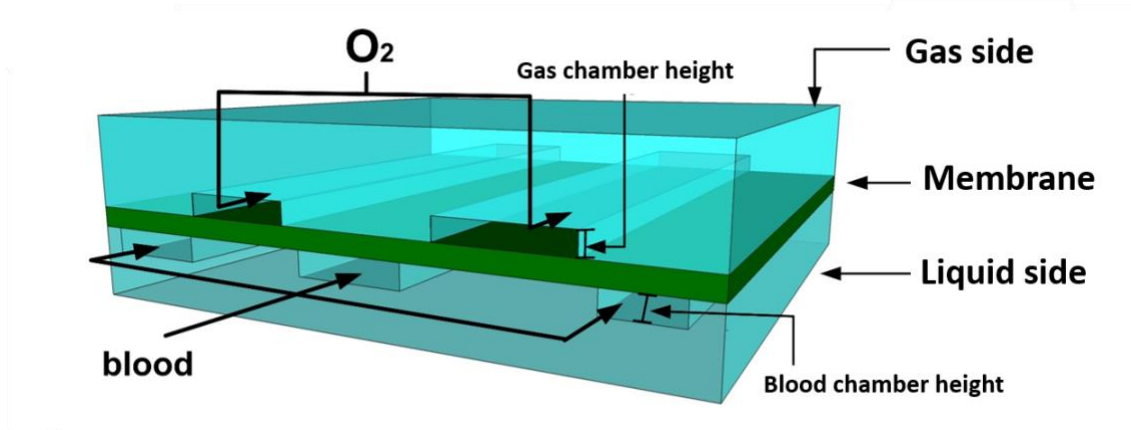


Figure 1 Schematic representation of the microfluidic artificial lung.

Along the last years, there was a remarkable advancement in the design and fabrication of the microfluidic devices for blood oxygenation. The silicon micromachining technology for replica moulding of PDMS for lung-on-a-chip, established by Borenstein *et al*, allowed to control the geometry and dimensions of the microfluidic platforms.^[21, 22] Currently, thanks to the progress of soft lithography, a broader variety of shapes, depths and lengths can be obtained and handled at the same time. The same group studied which criteria of various important parameters – i.e. shear stress, pressure drop and homogeneous liquid flow distribution – should meet in order to keep blood on a physiological level.^[22] A variety of branching human-lung-like geometries were obtained with regulated channel depth, width and length.^[23] In addition, one of the major milestones in the design and fabrication of a branched vascular system with minimal hydraulic losses (ΔP) was the architecture constructed by the group of Vacanti, offering different channel depths along the entire structure, i.e. 700 μm to 100 μm . Their procedure significantly decreased pressure drop and shear stress in the blood side.^[24] The group of Potkay designed a liquid chamber with shallow blood channels, i.e. 20 μm and 10 μm , respectively.^[25] It was concluded that shallower blood channels resulted in faster oxygenation,

because of the reduced pathway that oxygen needs to pass to bind to Hb, however, a rather high pressure drop was observed inside the liquid side of the device. Later, the same group demonstrated a blood chamber height of 30 μm as a trade-off to maximize oxygenation performance and to decrease the number of layers that are required for a clinically-relevant device.^[26] In a step further, Thompson et. al presented a new approach with a four-layer structure (blood layer/membrane/air layer/capping layer) that was assembled by rolling around a cylindrical substrate on the patterned PDMS substrate, thereby stacking the four layers.^[27] In 2018, Dabaghi et al. presented an artificial placenta type microfluidic blood oxygenator with double-sided gas transfer microchannels for neonates capable to oxygenate blood through exposure directly to ambient atmosphere without air pumping.^{[28], [29]} The ultra-thin device, with the total thickness below 300 μm , is flexible and compact thanks to the reinforcement of PDMS by porous PTFE scaffolds.^[30] Our group has recently designed and tested a meander type architecture with double-side vertical membrane arrangement where the oxygen and blood channels were fabricated in the same plane.^[31] Such arrangement presented not only double side gas diffusion, but also a simplified manufacturing process characterized by simple one-plane fabrication. However, our μAL based on this double-side vertical membrane configuration was subject to a relatively high pressure drop, i.e. 16.9 mbar at 1 mL/min blood flow rate which may result in thrombosis formation. Herein, it is useful to underline the potentialities of microfabrication techniques based on 3D printing to revolutionize the μAL technology by close mimicking of their natural counterparts.^[32]

Hence, the first part of the work is devoted to the Computational Fluid Dynamic (CFD) modelling of both alveolar-type architectures. It also comprises an optimization of the geometrical parameters of AD2-type devices to maintain the pressure drop and shear stress in the physiological range. In the second part, the fabrication and surface modification procedures for AD1 and AD2 microfluidic devices are briefly described, followed by the experimental methodology. Theoretical modelling of the oxygen transport is performed for both μAL designs

to support the experimentally obtained oxygen transfer rate values. Finally, a comparison with literature results, i.e. oxygen transfer rate, is provided. Moreover, there is an outlook on use of the alveolar devices for neonates taking into account the priming volume, and gas exchange surface area to satisfy their oxygenation requirements.

2. Numerical and Experimental Methods

2.1. Device design and optimization by computational fluid dynamics modelling

The microdevices herein studied consist of two chambers made of PDMS, where one is dedicated to gas and the other to blood, separated by a dense permeable membrane. In such arrangement, pure oxygen is introduced to the gas chamber of the device, permeates through the PDMS membrane into the liquid chamber, where it diffuses into the blood.

In particular, two different liquid geometries were investigated, i.e. alveolar design 1, denoted as AD1, based on the geometry reported by the group of Borenstein ^[16, 17, 23] and used as a reference, as well as alveolar design 2, AD2. This AD2 design is an improvement of AD1 in terms of fluid dynamics by modifying the distributors in contact with blood. As a consequence, the shear stress is notably decreased. The main purpose of such modification is to improve the blood compatibility.

The liquid chamber of AD1 is comprised of branching liquid channels with a depth of 100 μm . The structure consists of a big entrance, i.e. 2000 μm wide, with 4 main branches that contain 8 identical single units. Each unit possesses a set of parallel and perpendicular channels (see Figure 2). Within each unit ‘obstructions’ are present, which serve as flow distributor as well as prevent membrane deflection/collapse. The entrance and outlet of blood occurs through metallic pins with an angle of 90° (see Figure S1 in the Supplementary Information).

The complete liquid chamber, as well as a single unit were numerically analysed in 2D in COMSOL Multiphysics 5.0 software in terms of: liquid flow distribution, pressure distribution and shear stress exerted on the microchannel walls. A detailed description of the computational fluid dynamics model can be found in our previous work.^[31] The mesh-size used in the

simulations was chosen on the basis of computational costs and reproducibility of hydrodynamic results. On this regard, the 2D computational domain for the reference AD1 design was discretized by more than 160 000 triangular elements, with a mesh of an edge length in the range 3000 μm to 16 μm .

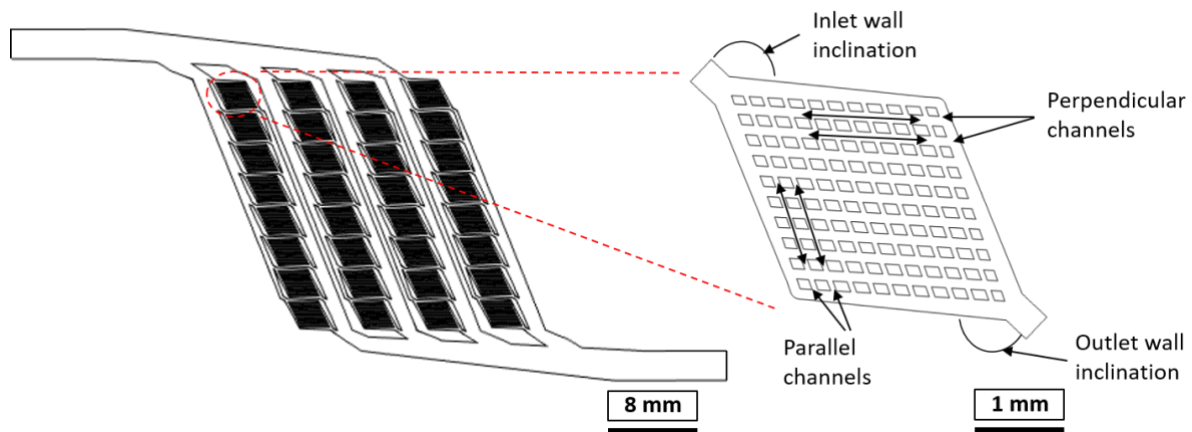
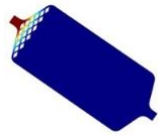
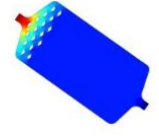
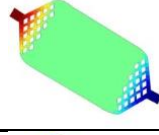
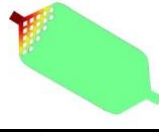
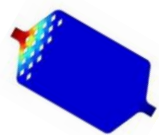


Figure 2 Liquid chamber architecture and magnified single unit of reference AD1-type design.

A variety of computer simulations with different single unit configurations (see Table 1) was performed in attempt to optimize the alveolar type geometry and identify the most appropriate unit architecture for blood oxygenation testing. Aim of the proposed modifications was to decrease ΔP and shear stress of the liquid chamber, while maintaining a homogeneous flow distribution and high level of oxygen transfer rate as well as minimizing chamber size and the number and organization of distributors at the same time. Basically, within the unit of design AD2, the perpendicular and parallel channels in AD1 were removed, and flow distributors were incorporated in the reservoir.

Table 1 Proposed AD2-type single unit configurations for fluid dynamics optimization.

Design	Description*	
AD2-1	Single side distributor, 20 μm spacing, diamond shape; approx. 100° inlet angle; 1450 μm reservoir width	
AD2-2	Single side distributors 100 μm spacing, diamond shape; approx. 100° inlet angle; 1450 μm reservoir width	
AD2-3	Double side distributors, 50 μm spacing, diamond shape, approx. 130° inlet angle; 1750 μm reservoir width	
AD2-4	The same as design 3, but single side flow distributor	
AD2-5	Single side distributor, 130 μm spacing, diamond shape; 130° inlet angle; 1750 μm reservoir width	

*The graphical representation of each design shows the results of the pressure drop CFD simulation at 1 mL/min blood flow rate (see Section 3.1)

In addition, the liquid channels were initially designed to obey the bifurcation theory introduced by Murray in 1926.^[33] Thus, whenever the channel bifurcates or trifurcates the width must always be 1/2 or 1/3 of the width of the original main channel so the homogenous liquid distribution is kept. However, the Murray's law was finally not followed, and the dimensions of the daughter vessels were increased in some sections of the single unit to avoid the out-of-range pressure drop values indicated by CFD simulation. It is important to mention that to keep the blood at a physiological level a crucial restriction of the shear stress values needed to be obeyed. Shear stress should not exceed the normal range in the human vascular system which varies from 0.1 to 7 N/m².^[24] Therefore, the following parameters were analysed in more detail:

1) shape and dimensions (length and width) of the reservoir, 2) flow distributors: shape, size, position and in-between spacing and 3) inclination angle of the walls near the inlet and outlet of the reservoir.

2.2.Oxygen transport model

The blood oxygenation process in a single unit was studied in detail for both alveolar type geometries for a more comprehensive understanding. The standard convection-diffusion mass transfer expression was used to develop the mass balance and transport equation for oxygen species in blood.^[34-36]

The coupling between the oxygen mass balance in blood plasma and the membrane surface is obtained as a boundary condition in the liquid's mass balance. This condition sets the flux of oxygen at the boundary equal to the permeation rate through the PDMS membrane. For more details about the oxygen transport model, we refer to our previous work.^[31]

2.3.Microfluidic oxygenation devices: fabrication process and basic characterization

Three different microfluidic devices of each design, AD1 and optimized AD2 (AD2-5, see section 3.1), were fabricated in polydimethylsiloxane (PDMS; Sylgard 184 Dow Corning, Midland, MI) and applied for blood oxygenation. The PDMS was chosen due to its highly elastic properties, transparency, high gas permeability, biocompatibility and easiness in releasing from moulds which characterizes a good material for replica moulding.^[31] The fabrication process involved: 1) construction of liquid and gas chambers by replica moulding from rigid masters, 2) membrane fabrication and 3) microdevice assembly and attachment (see Figures S1-S2 in SI). The detailed fabrication description can be found in.^{[37] [17, 38]}

The membrane thickness (120 μm) as well as the channel depth (100 μm) were identical for both designs and similar to our previous work.^[31] For this work, mainly focused on the liquid chamber geometry, the membrane thickness was chosen to stay on the safe side and to avoid additional obstacles in the microdevice fabrication. Above all, and based on our microfabrication experience, the further reduction of the membrane thickness would not introduce any complexity to the easy to fabricate approach based on straightforward PDMS-casting and release.

The μAL -footprint, defined as the total areal size of the microfluidic device, was equal to 18.7 cm^2 . The volume of the gas chamber was equal to 73 μL for both device types, the volume of the liquid chamber (without microfluidic connections) and membrane surface area are 28 μL and 2.8 cm^2 for AD1 and 39 μL and 3.9 cm^2 for AD2-5, respectively. Thus, the gas exchange surface area is approximately 40% higher in case of AD2-5. In both designs, a number of supporting pillars were added to the gas chamber to avoid membrane collapse/bending and to increase the mechanical stability of the devices (which didn't influence the flow distribution). Accordingly, the effective gas exchange surface areas used for the estimation of the oxygen transfer rate are 2.25 cm^2 for AD1 and 3.32 cm^2 for AD2-5, respectively. Thus, the effective gas exchange surface area is approximately 47% higher in case of AD2-5, resulting in a higher surface (effective gas exchange surface area) to volume (total chip volume) ratio.

Figure 3 comparatively shows an AD1 and an AD2-5 microfluidic device of which the liquid chambers are filled with blood (including two magnifications). The images indicate that the filling of the liquid channels was homogeneous, and well-distributed without spots with stagnant air, non-moving air bubbles or non-wetting spots. It was of crucial importance to confirm that the membrane which is "sandwiched" in-between the liquid and gas chambers did not deflect, collapse, rupture or detach. Figure 4 shows SEM images of the cross section of the two microdevices, which illustrate that the membrane was well attached to the microfluidic

chambers in both cases. No leakage was observed, and each device was capable of working for a long time, i.e. more than 8 hours, under the experimental conditions. The experimental set-up with the microfluidic devices can withstand liquid flow rates up to 5 mL/min. In other words, the devices were able to operate for at least 8 hours at a blood flow rate up to 5 mL/min without experimental evidence of either channel collapse, blockage or thrombus formation.

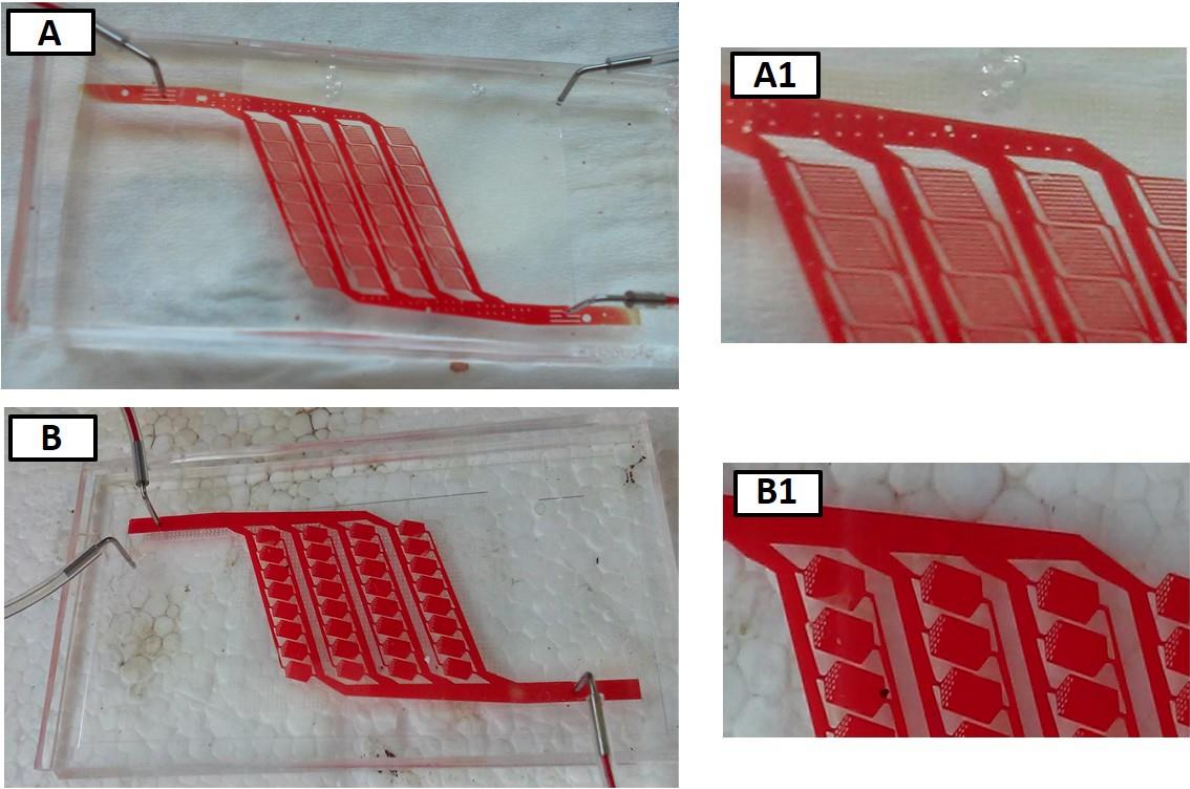


Figure 3 Optical images of A) AD1 and B) AD2-5 PDMS microfluidic devices with sheep blood inside the liquid chamber. A1 and B1 are the magnifications of AD1 and AD2-5, respectively.

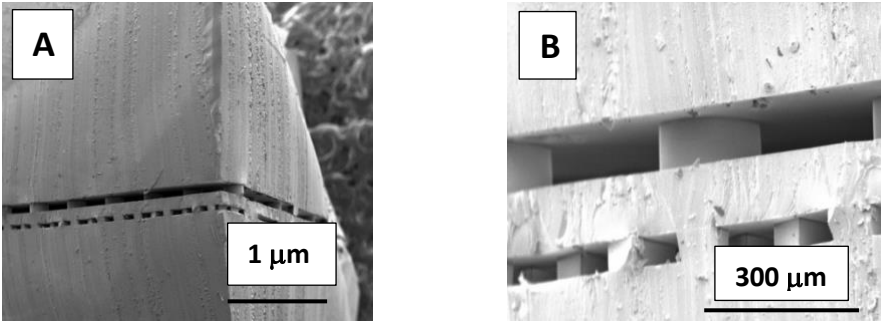


Figure 4 Cross-sectional SEM images of A) AD1 and B) AD2-5 type microdevices studied in this work.

Metallic pins (precision stainless steel dispense tips from Nordson, The Netherlands) with an outer diameter of 0.025” and gauge 23 were inserted at the inlet and outlet of the gas and liquid chambers to facilitate connection of the tubing to the device to flow gas and blood into the chambers. The volume of these connectors is circa 1.1 μ L each.

In artificial lung assist devices, the adhesion of red blood cells is highly undesired to avoid membrane fouling and blockage of blood channels. Hydrophilic surfaces are commonly preferred due to less protein unfolding.^[39, 40] Therefore, the blood contacting surface was coated with Pluronic F-68 to render it more hydrophilic (a detailed description can be found in Supplementary Information, specifically in Figures S3 – S6 and Table S1). Prior to the blood oxygenation experiments, the surface of the modified PDMS microdevices and fibrinogen adhesion were investigated to assess on hemocompatibility (see Figure S4 and Figure S5 in SI). Moreover, the sample of blood after the oxygenation experiments (maximum 24 hours after) was analysed to corroborate the functionality of RBCs (see Figure S6 in SI and Table S1 in SI).

2.4. Blood oxygenation experimental set-up

The experimental system as well as the protocol for blood oxygenation were the same as in our previous work.^[31] Briefly, all the oxygenation experiments were carried out with sheep blood obtained from the Faculty of Veterinary of the University of Zaragoza with ethylenediaminetetraacetic acid (EDTA) as anticoagulant in a concentration of 1.5 mg/mL (standard value of commercial blood collection tubes). Blood was stored under refrigeration at 4° C during a maximum period before essays of 24 hours. The concentration of haemoglobin differed slightly from sample to sample. Therefore, for each experiment the Hb concentration was measured by gasometry (Vet abc Classic, Animal Blood Counter) before and after each oxygenation experiment (see Table S1 of the SI). The main blood inlet parameters for each oxygenation experiment are shown in Table S2.A of the SI. 50 mL of blood was placed in a climatic chamber at 37°C and a mixture of air and nitrogen with 7.8% of O₂ was bubbled

directly to the blood, in order to decrease the O₂ blood saturation down to approximately 60-80%. The blood was pumped in the μ AL at blood flow rates ranging from 0.1 to 5 mL·min⁻¹ and continuously measured and kept at the targeted rate. The pressure drop across the entire system (considering the metallic pins, tubing and the microdevice itself) was continuously monitored by a pressure transducer (Panasonic, DP2-41E) that was placed directly after the syringe pump. It is noted that during operation of the μ AL the blood flow rate and pressure are continuously monitored to sense/detect potential clotting in the device. Subsequently, the deoxygenated blood entered the liquid chamber of a microdevice, while the gas chamber was purged with pure oxygen. The initial volume of outlet blood stream (2 mL) was discarded to ensure steady state conditions and that all the blood passed through the device, metallic pins as well as all the piping in the system. Various parameters were measured and controlled such as: pH, temperature and the amount of oxygen in blood. It was done by immersing a pH electrode (Hamilton, Slimtrode 238150, Switzerland) and a dissolved oxygen electrode, type oximeter (ThermoFisher Scientific, Orion Star A223) in a glass bottle that was hermetically sealed. An oximeter measures the dissolved oxygen in blood plasma, and the oxygen partial pressure (P_{O₂}) is directly calculated assuming Henry's law, i.e. a constant solubility for a given temperature, pH and P_{CO₂}. Due to oxygenation temperature variations among different tests, the oxygenation performance for a given conditions was evaluated from the equivalent P_{O₂} values, i.e. those expressed at standard conditions (37°C, pH of 7.4 and P_{CO₂} of 40 mm Hg). A control sample measurement was performed before each set of experiments to ensure neither leaks of the system nor blood oxygenation by the oxygen stored in the head space of the blood collecting bottle.

For each identical microfluidic device, three repetitions were performed at distinctive blood flow rates to assess repeatability (see Table S2.A in SI for the main parameters of each of the oxygenation experiments).

The evaluation of the oxygenation performance of the microdevices is assessed by the oxygen transfer rate $O_{2transf}$ ($\text{mL}\cdot\text{m}^{-2}\cdot\text{min}^{-1}$) through the PDMS membrane, calculated according to the equation 1:

$$O_{2transf} = \frac{\alpha \cdot \Delta P_{O_2} + Hbs \cdot \Delta S_{O_2} \cdot [Hb]}{S_A} \cdot Q \quad (1)$$

where: α is the solubility coefficient of O_2 in blood plasma, ΔP_{O_2} [mbar] is the difference between the outlet and inlet experimental values of partial pressure that corresponds to the dissolved oxygen measured, ΔS_{O_2} is the increment in oxygen saturation in blood, Hbs is the O_2 binding capacity of haemoglobin, $[Hb]$ is the haemoglobin concentration in blood, Q is the blood flow rate and S_A is the effective gas exchange surface area. The term $Hbs \cdot \Delta S_{O_2} \cdot [Hb]$ corresponds to the variation in the concentration of oxygen in blood that is bound to haemoglobin.

The term $\alpha \cdot \Delta P_{O_2}$ corresponds to the variation of the concentration of dissolved oxygen in plasma. The fractional saturation of blood (S_{O_2}) is calculated according to Hills equation:^[34]

$$S_{O_2} = \frac{\left(\frac{P_{O_2}}{P_{50}}\right)^n}{1 + \left(\frac{P_{O_2}}{P_{50}}\right)^n} \quad (2)$$

Where: P_{O_2} is the partial pressure of dissolved oxygen (experimentally obtained), n is the number of binding sites of haemoglobin (called the Hill coefficient); and P_{50} is the partial pressure of oxygen when blood is 50% saturated. Please refer to Table S3 in SI for the main blood and oxygen related parameters used in the calculations.

3. Results and discussion

3.1. Fluid dynamics simulation of alveolar-like microfluidic devices

The liquid flow velocity, pressure and shear stress distributions for the entire liquid chamber architecture and for a single unit of AD1 microfluidic device are depicted in Figure 5. The pressure drop and shear stress at 1 mL/min blood flow rate were 2.57 mbar and 7.93 N/m², respectively. The chosen single unit for the magnified profiles was the first unit in the first branch of the entire structure, because this is the unit experiencing the highest ΔP and shear stress. The arrangement of the perpendicular and parallel channels of the AD1 single unit leads to preferential pathways at the peripheral of the unit, where the highest shear stress values are registered (see Figure 5 C1).

Similarly, Figure 6 shows the pressure distribution at 1 mL/min blood flow rate for some of the proposed AD2 single unit architectures. The calculated pressure drops and maximal shear stress values for unit configurations shown in Figure 6 A and B are 7.65 mbar - 28.2 N/m² and 3.36 mbar- 8.25 N/m², respectively. The high ΔP in Figure 6 A is related to the small spacing of 20 μm between the diamonds composing the flow distributor. A larger spacing between the diamonds, i.e. 100 μm as presented in Figure 6 B, decreases the pressure drop by approximately a factor 2, which is still higher than the value of the AD1 unit. This is due to the width-dimension of the reservoir, i.e. 1450 μm (which seems to be too narrow), as well as the angle of the tapered channel transition at the inlet, i.e. inlet/outlet wall inclination (approximately 100°). A lower value of the inclination angle results in a sharper cross-section change, leading to elevated ΔP values.

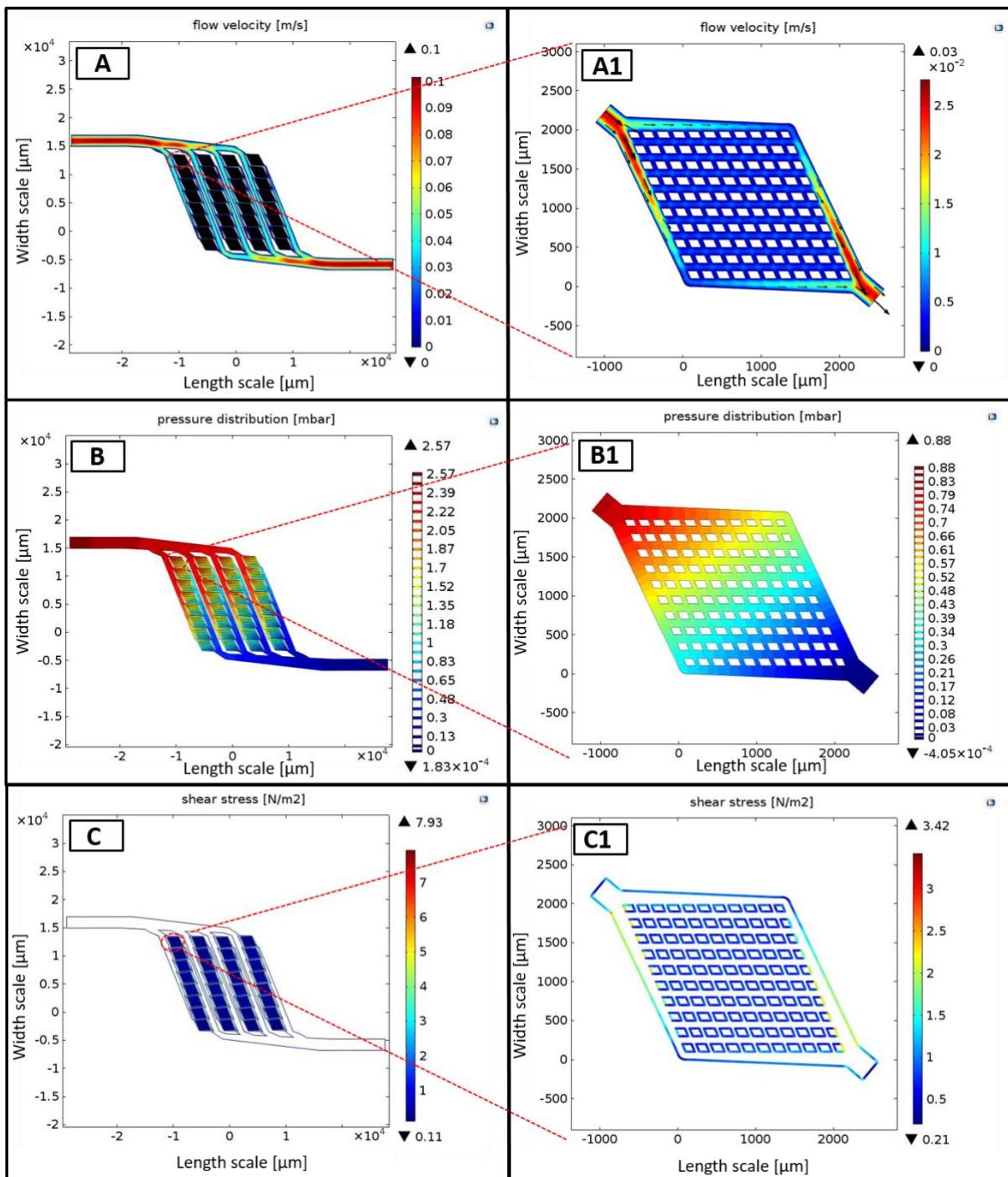


Figure 5 CFD computational results of A) flow velocity, B) pressure distribution and C) shear stress for a blood flow rate 1 mL/min in AD1. A1, B1 and C1 represent the magnifications of the first single unit.

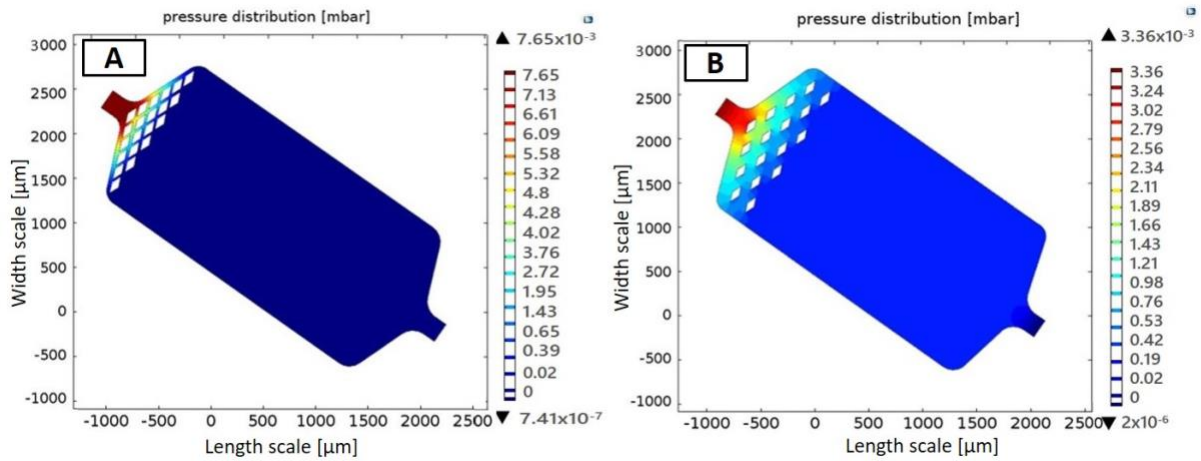


Figure 6 Simulation results of pressure distribution of single units with different configurations/designs (see Table 1) for a blood flow rate 1 mL/min: Design AD2-1 (left) and Design AD2-2 (right).

As a result of AD2-1 and AD2-2 computer simulations, it was decided to increase the width of the single unit reservoir from 1450 μm to 1700 μm and to increase the inclination/taper angle from 100° to 130°. Figure 7 shows the computer simulation of a single unit slightly wider in size (ca. 15%), and with a larger taper/inclination angle at the inlet (and outlet), i.e. approximately 130°, as well as identical liquid flow distributors at the inlet and outlet of the reservoir. The calculated pressure drop and maximal shear stress values for design AD2-3 at 1 mL/min blood flow rate are 1.82 mbar – 6.62 N/m^2 , i.e. significantly lower than of designs AD2-1 and AD2-2. An identical unit-layout with only a flow distributor at the inlet, AD2-4 was simulated as well, which yielded a further reduced pressure drop and shear stress values, i.e. 1.22 mbar – 6.37 N/m^2 . Therefore, single units with only a flow distributor at the inlet were considered as being the best choice. Accordingly, design AD2-5 was chosen as the most efficient geometry, among the tested, for the unit to be implemented in the liquid chamber of a microfluidic device for blood oxygenation experiments (see Figure 8 for the layout).

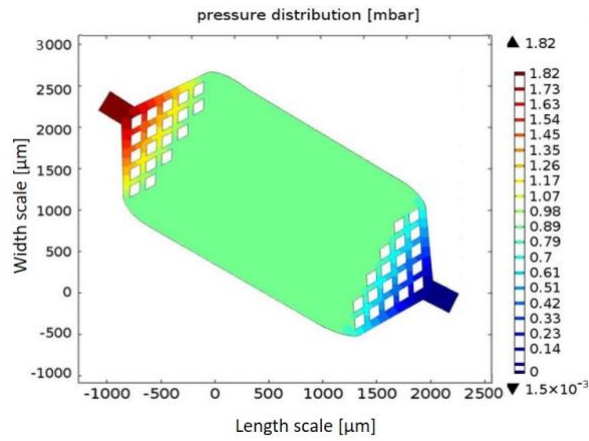


Figure 7 CFD computational result of pressure distribution for a single unit of design AD2-3 and Design AD2-4 (see Table 1) with flow distributors at the inlet and outlet for a blood flow rate 1 mL/min.

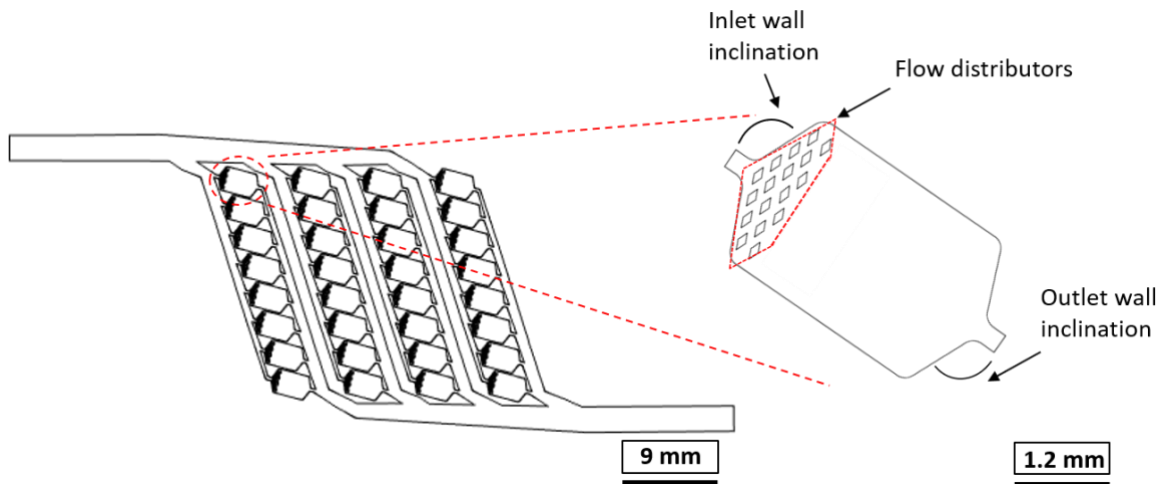


Figure 8 Liquid chamber architecture and single unit magnification of the optimal AD2-5 design.

The liquid flow velocity, pressure distribution and shear stress for this AD2-5 geometry were simulated (see Figure 9). The final mesh used in computer simulations consisted of more than 780 000 triangular elements, defining a mesh with an edge length in the range 4000 μm to 17 μm . It is clear that the pressure drop is significantly reduced, by approximately a factor 4 to 0.64 mbar for AD2-5 (2.57 mbar for AD1), mainly due to removal of horizontal and vertical microchannels in the reservoir. Moreover, the maximum shear stress decreased as well from 7.93 N/m^2 (AD1) to 4.7 N/m^2 for AD2-5. The flow velocity profile depicted in Figure 9.A1 shows areas of low flow close to the walls that could eventually result in stagnation and

accumulation of pro-coagulation factors. However, in these regions the shear stress is also low (see Figure 9 C1) and in the range of physiological shear (not exceeding 7 N/m^2). In addition, the visual inspection of the fabricated microdevices after 8 hours blood testing (see Figure S4 in the SI) did not reveal any clotting. We attribute this behaviour to the modification of the PDMS surface (for the detailed description refer to Section 2 of the SI).

The shear-induced and material induced blood trauma factors, $T_{F,S}$ and $T_{F,M}$, respectively, were analysed for 1 mL/min blood flow rate according to the model of Mockros and Cook ^[41] (see our previous work ^[31] for detailed calculation). In general, the $T_{F,S}$ should be lower than zero and $T_{F,M}$ should be greater than zero to avoid blood trauma. Calculated $T_{F,S}$ values from the average shear stress data are -606.2 and -607.4 for AD1 and AD2-5, respectively, and this supports the absence of shear-induced platelet activation. On the contrary, $T_{F,M}$ values are -11.4 and -12.9 for AD1 and AD2-5, respectively. These values would indicate that the material-induced blood trauma due to stagnation could be present. However, as stated before, we did not record any accumulation of activated coagulation factors in the structure along the blood oxygenation experiments.

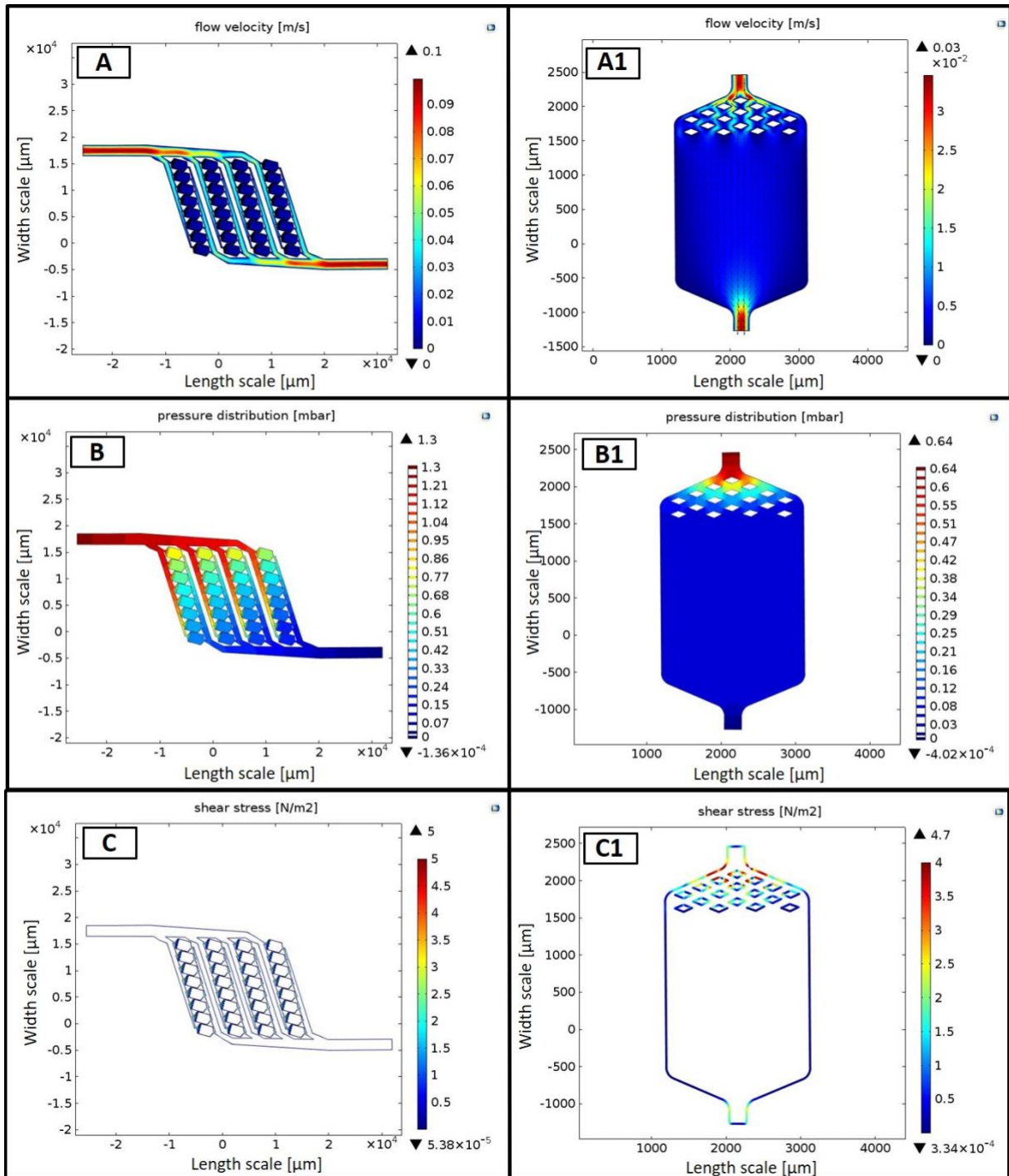


Figure 9 CFD computational results of A) flow velocity, B) pressure drop and C) shear stress for a blood flow rate 1 mL/min in AD2-5. A1, B1 and C1 represent magnifications of a single unit.

3.2. Simulation of blood oxygenation in a single unit of alveolar-like microfluidic devices

In Figure 10 and Figure 11 the simulated oxygen concentration profiles are shown for two liquid flow rates: A) 0.1 mL/min ($Re=0.30$) and B) 1 mL/min ($Re=3.02$), along a single unit of AD1 and AD2-5 devices, respectively. The predicted O_2 concentration values, expressed in mol/m^3 , correspond to the total oxygen concentration in blood (i.e. oxygen bound to haemoglobin + dissolved oxygen). The average value for the total oxygen concentration at the outlet of the single unit is calculated by numerical integration across the transversal section of the liquid channel.

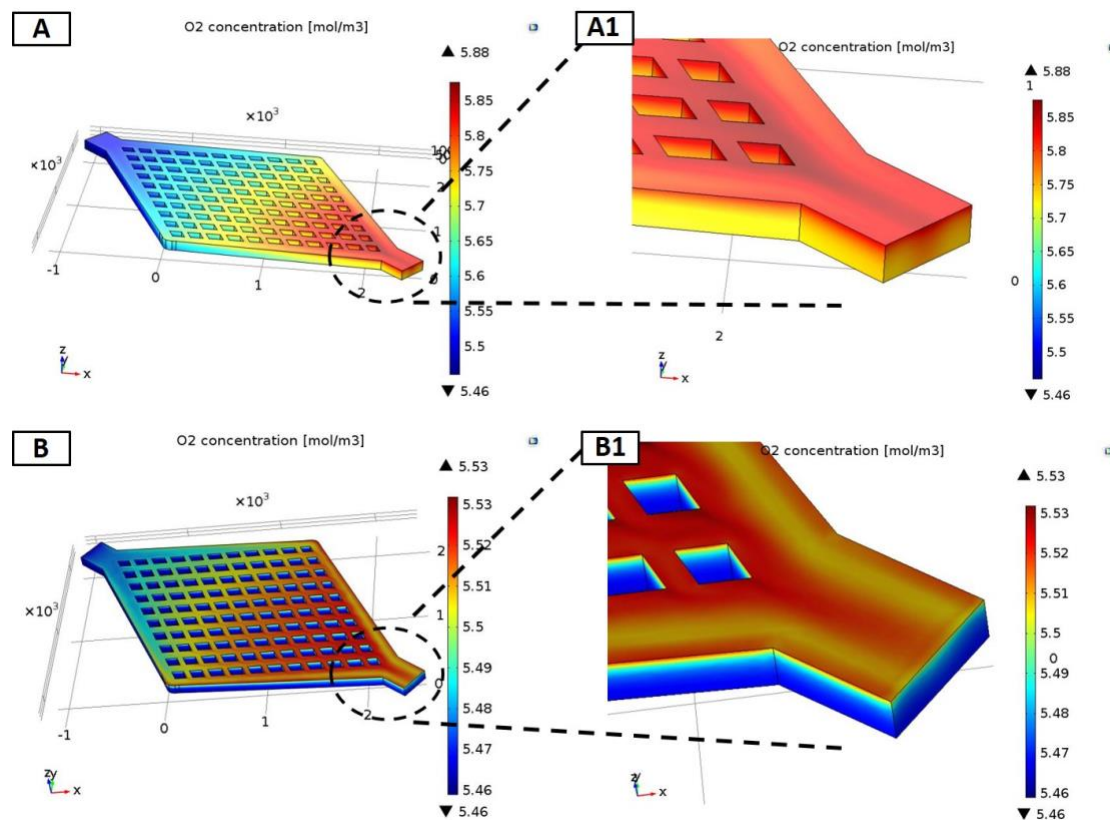


Figure 10 Oxygen concentration profile by computer modelling of a single AD1 unit at A) 0.1 mL/min and B) 1 mL/min blood flow rates, respectively.

At a low blood flow rate, oxygen can diffuse deeper into the liquid chamber, resulting in a higher concentration of oxygen at the outlet of a single unit. The calculated average values for

AD1 are 5.75 mol/m^3 (69.1% SO_2) and 5.48 mol/m^3 (65.8% SO_2) at 0.1 mL/min and 1 mL/min blood flow rate, respectively.

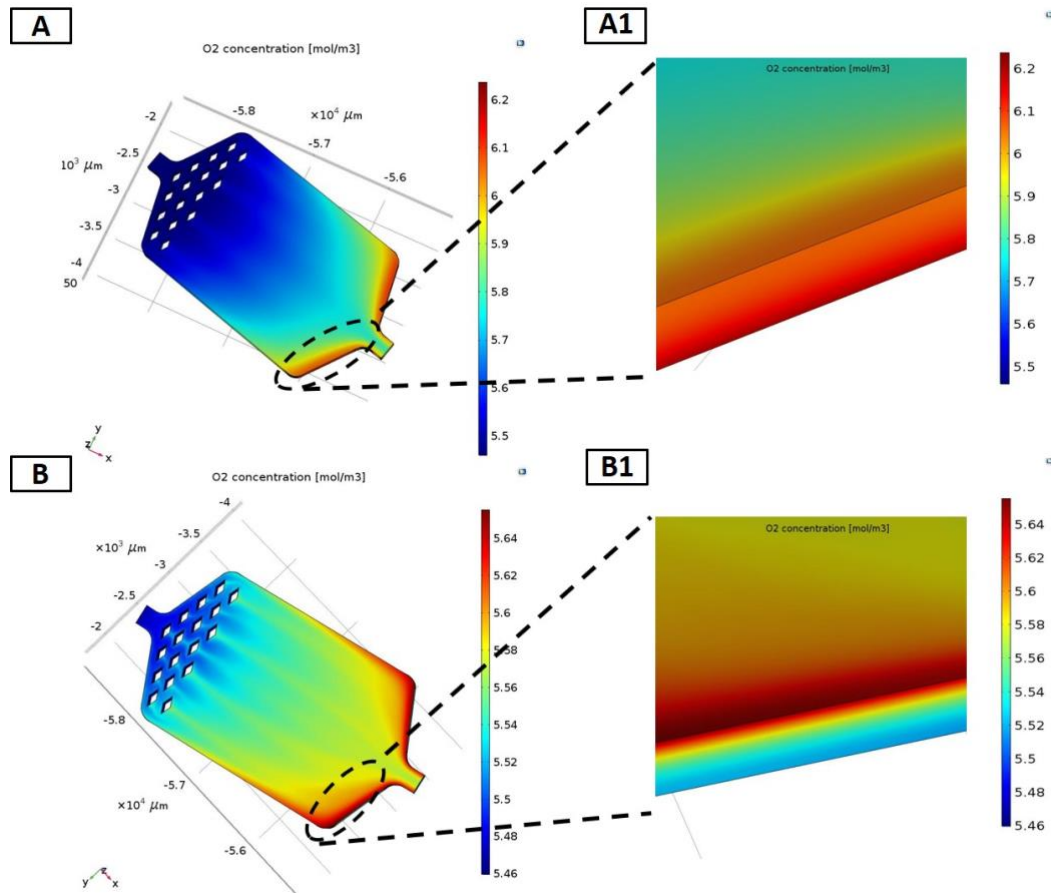


Figure 11 Oxygen concentration profile by computer modelling of a single AD2-5 unit at A) 0.1 mL/min and B) 1 mL/min blood flow rates, respectively.

The same analysis is also performed for design AD2-5 (Figure 11). The AD2-5 unit exhibits high oxygen concentration values at the corners near the walls situated close to the outlet due to its distinctive geometrical features (outlet angle 130°). The gas exchange efficiency is slightly better for a AD2-5 single unit (compared to an AD1 unit), rendering in higher value for the average concentration of oxygen at the outlet, i.e. 5.90 mol/m^3 (70.9% SO_2) and 5.53 mol/m^3 (66.4% SO_2) at 0.1 mL/min and 1 mL/min blood flow rate, respectively. This is in agreement with experimental data (Figure 12 and Figure 13). Overall, it can be seen that the

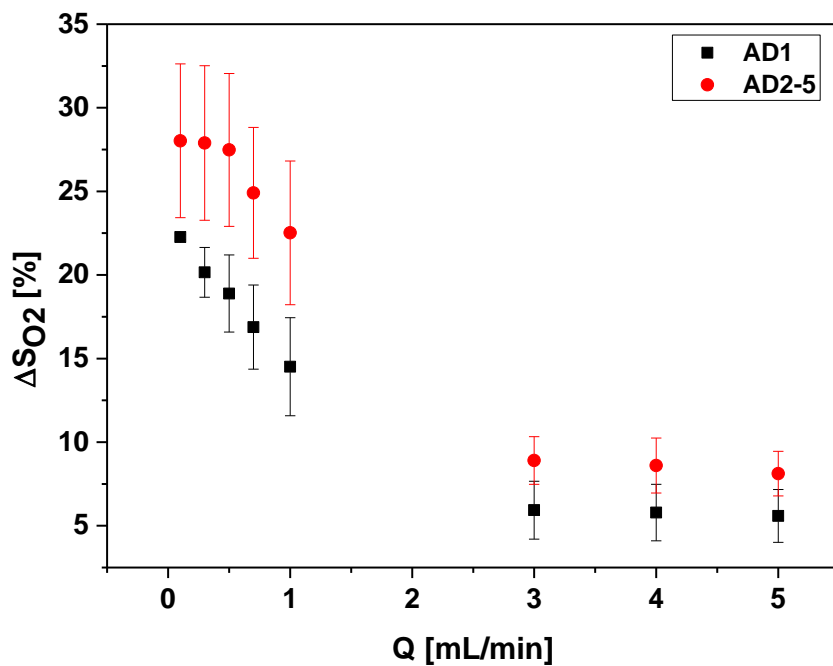
AD2-5 design exhibits not only a lower ΔP , but has also a slightly better oxygenation performance.

3.3. Experimental blood oxygenation performance of alveolar-like microfluidic devices

Figure 12A illustrates the evolution of the oxygen saturation level, expressed as variation from the starting value, as a function of the blood flow rate for both AD1 and AD2-5 devices, respectively. Such representation helps to rapidly visualize the operational working conditions to satisfy the oxygenation requirements. The error bars represent the standard deviation of three repetitions of the same measurement (see Table S2.A and Table S2.B in SI for details of each experiment). The O_2 saturation level decreases in a nonlinear fashion as the blood flow rate increases. The steepest part of the curve occurs at a blood flow rate ranging from 0.1 to 1 mL/min, while (almost) a plateau is attained at flow rates ≥ 2 mL/min. Additionally, the AD2-5 device shows a slightly better oxygenation performance for a given blood flow rate than AD1, i.e. 22.50 ± 4.30 versus 14.51 ± 2.93 of incremental ΔS_{O_2} at 1 mL/min for AD2-5 and AD1, respectively.

Figure 12B shows the experimentally measured pressure drops for the microdevices AD1 and AD2-5 as a function of the blood flow rate. It also includes the theoretical pressure drops (dashed lines) as determined by computational calculations. Considering the arteriovenous differential pressure for a neonate is between 26.7 and 80 mbar,^[28] we have taken the lowest value (i.e. 26.7 mbar) as the maximum pressure drop that can be tolerated for the microdevices prepared in this work (dotted line in Figure 12 B). From the experimental results, it can be concluded that both architectures fulfil this criterion for the investigated flow rate range, and that the AD2-5 device demonstrates the lowest pressure drop (in accordance with the CFD simulations) without a negative effect on the oxygenation level.

A)



B)

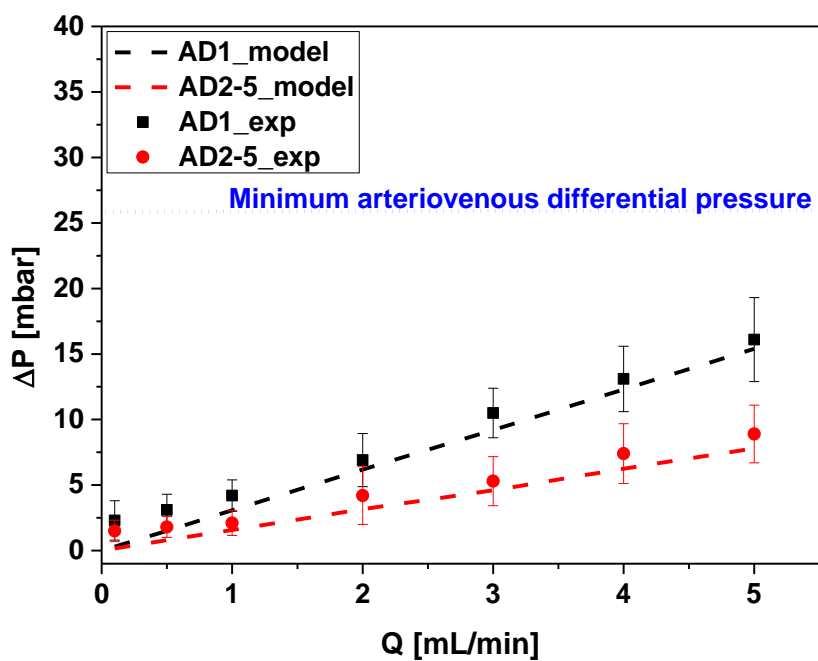
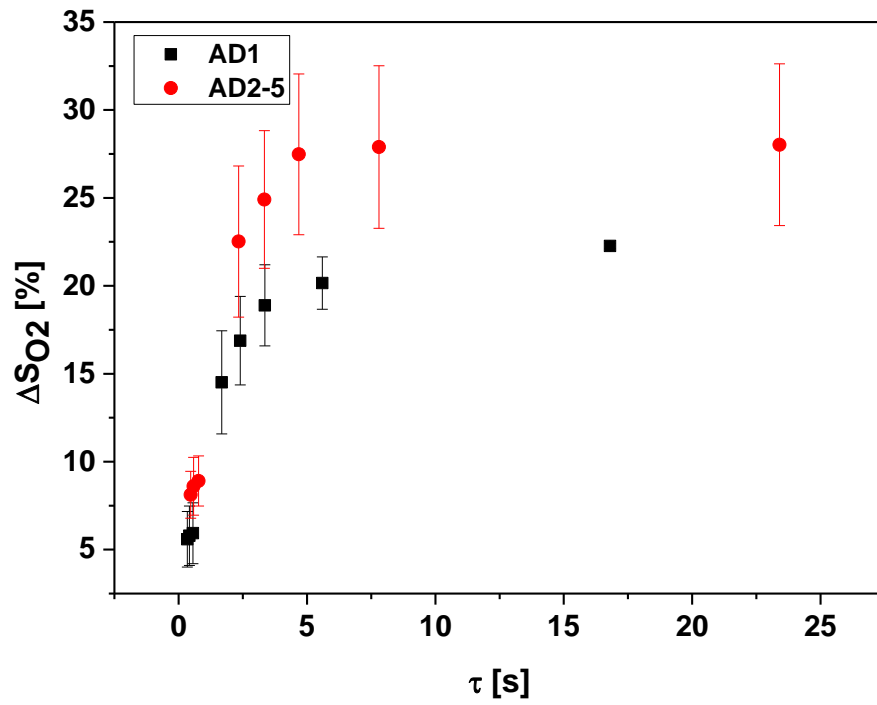


Figure12. Oxygen Saturation in blood, expressed as incremental ΔSO_2 , A) and experimental pressure drop values B) as a function of the blood flow rate for AD1 and AD2-5 microdevices.

A)



B)

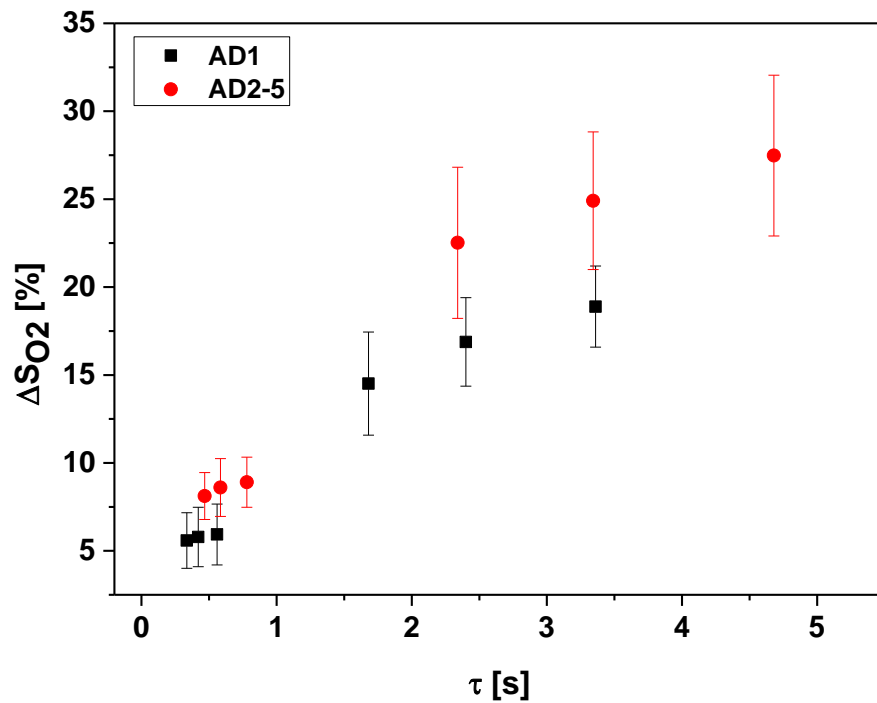


Figure 13 Oxygen Saturation in Blood, expressed as incremental ΔSO_2 , as function of residence time (τ) for AD1 and AD2-5 type microdevices for the A) entire range of liquid flow rates and B) magnification when operating at the lowest τ .

To discard any differences of the nominal liquid chamber volume in both microfluidic designs, Figure 13 shows the changes in oxygen saturation as a function of the residence time (τ) for both designs. For lower τ values, i.e. higher blood flow rates, a linear dependence is observed. As the blood flow decreases (i.e. τ increases), the incremental oxygenation saturation eventually levels off due to approaching reaction completion, i.e. a 100% oxygen saturation level (circa 33% for the incremental value). As previously shown in Figure 12, the AD2-5 device shows a slightly better oxygenation performance for a given residence time.

Figure 14 shows the gas exchange, expressed as oxygen transfer rate ($\text{mL}\cdot\text{m}^{-2}\cdot\text{min}^{-1}$) as a function of the blood flow rate normalized per effective gas exchange surface area ($\text{mL}\cdot\text{m}^{-2}\cdot\text{min}^{-1}$). Such plot enables a fair comparison of the experimental oxygenation performance with data from other microfluidic devices designed to operate at specific flow rates. For the devices presented in this work, the gas exchange increases with the blood flow rate but the increment is not linear, as the $\Delta\text{S}_{\text{O}_2}$ dependence (see equation 2).

It is clear that the oxygenation performances of our proposed alveolar designs are among the highest values reported in the literature. At a blood flow rate of 1 mL/min, the oxygen transfer rate for our two designs is $123 \text{ mL}\cdot\text{m}^{-2}\cdot\text{min}^{-1}$ (0.028 mL/min) and $127 \text{ mL}\cdot\text{m}^{-2}\cdot\text{min}^{-1}$ (0.042 mL/min) for AD1 and AD2-5, respectively: only the results obtained by the group of Borenstein ^[23] are better at this blood flow rate (i.e. $223 \text{ mL}\cdot\text{m}^{-2}\cdot\text{min}^{-1}$).

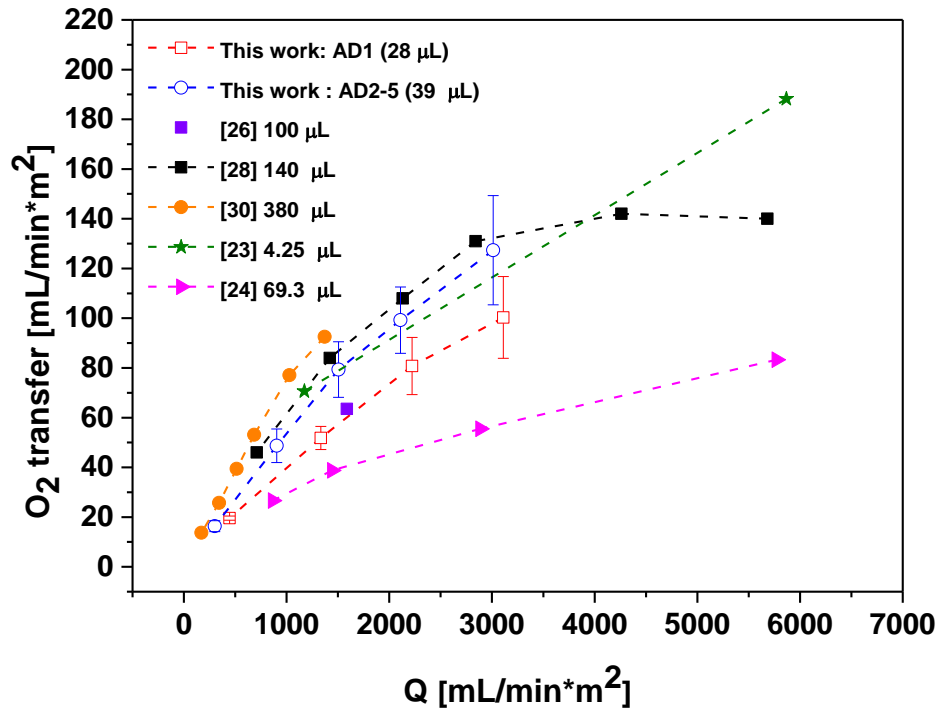


Figure 14 Oxygen transfer rate at various liquid flow rates for two geometries (AD1 and AD2-5) in comparison to literature results. The specified values refer to the liquid chamber volume of the microdevices. All literature references are with O₂ as a source gas.

Both AD1 and AD2-5 architectures exhibit a low pressure drop to blood flow ratio (see Figure 12), which is clearly beneficial for pumpless clinical applications, that enhances the portability and compactness of the oxygenation device. Both microfluidic devices represent an opportunity for decreasing the priming volume, which is especially relevant for blood oxygenation in the case of neonates. Considering that the rated blood flow, defined as the maximum flow rate at which blood with an inlet S_{O₂} of 75% is raised to 95% by the device, is the parameter commonly adopted for devices inter-comparison, Table S2.B in the SI shows that design AD2-5 data satisfies this for certain (highlighted in bold) conditions. In fact, the rated blood flow is 0.5 mL/min for the AD2-5 alveolar type design. Considering that the extracorporeal bypass volume is 30 mL·kg⁻¹·min⁻¹,^[10] our oxygenator was scaled to a rated

blood flow of 60 mL/min. This value is an approximate minimum required for neonate applications. In order to satisfy the oxygenation of a 2.0 kg infant, the volume of the liquid chamber and the gas exchange surface area of the AD2-5 μ AL (with 100 μ m deep liquid channels and a 120 μ m thick membrane) should approach 5 mL and 0.05 m² i.e. 120 chips stacked or operated in parallel. Such numbers are rather similar to those already reported in,^[16] although the pressure drop exhibited by the AD2-5 device is considerably lower. Moreover, if we take into account the commercial oxygenators for infants, the priming volume (without including fluidic connections and flow distributors) of our stacked AD2-5, i.e. 5 mL, is lower than the liquid volume of the oxygenators based on microporous hollow fiber membrane contactors. For example, QUADROX-I Neonatal and QUADROX-I Pediatric possess 38 and 81 mL volumes, respectively.^[42]

4. Conclusions

Compact and simple alveolar type microfluidic devices with a horizontal membrane arrangement and 100 μ m deep liquid channels have been developed. The footprint of both μ AL-devices is 18.7 cm². The volume of the gas chamber is 73 μ L for both device types, the volume of the liquid chamber (without microfluidic connections) and effective gas exchange membrane surface area are 28 μ L and 2.25 cm² for AD1 and 39 μ L and 3.32 cm² for AD2-5, respectively. Computer simulations in COMSOL Multiphysics 5.0 have enabled improvement of the alveolar design to maintain hydraulic resistances far below the limits for clotting and thrombus formation without affecting high oxygenation levels. At a blood flow rate of 1 mL/min the oxygen transfer rate for our two designs is 123 mL·m⁻²·min⁻¹ and 127 mL·m⁻²·min⁻¹ for AD1 and AD2-5, respectively. The blood oxygenation performance of the μ AL devices compares to the configurations reported in literature. Both architectures exhibit a low hydraulic resistance: a distinctive feature of pumpless clinical applications where circuit complications are reduced.

In order to satisfy the oxygenation requirements of 2.0 kg neonate and considering that its total blood volume is around 95-100 mL/kg, the estimated volume of a blood chamber in our scaled μ AL is less than 5 mL (that is well below 3% of its total blood volume).

Apart from the improvements herein demonstrated in the 2D vascular design of the oxygenator, it is clear that there is still room for further technological developments of μ ALs. Innovative ways to fabricate scaled microfluidic systems with simplified circuitry and improved haemocompatibility would revolutionize future devices and could lead to an improved life of patients.

Conflicts of interest

Authors declare that there are no conflicts of interest.

Acknowledgements

The authors would like to acknowledge the financial support from the Government of Aragon and the Education, Audiovisual and Culture Executive Agency (EU-EACEA) within the EUDIME – “Erasmus Mundus Doctorate in Membrane Engineering” program (FPA 2011-0014, SGA 2012-1719, <http://eudime.unical.it>). CIBER-BBN is an initiative funded by the VI National R&D&i Plan 2008–2011 financed by the Instituto de Salud Carlos III with the assistance of the European Regional Development Fund. Furthermore, the authors acknowledge the LMA-INA for offering access to their instruments and expertise.

References

1. R. R. Thiagarajan, R. P. Barbaro, P. T. Rycus, D. M. McMullan, S. A. Conrad, J. D. Fortenberry and M. L. Paden, *ASAIO*, **2017**, 60-67.
2. G. P. Gravlee, R. R. Davis, M. Kurusz and J. R. Utley, *Lippincott Williams&Wilkins*, **2000**.
3. K. J. Rehder, D. A. Turner, D. Bonadonna, R. J. Walczak, R. J. Rudder and I. M. Cheifetz, *Expert Review of Respiratory Medicine*, **2012**, *6*, 377-384.
4. J. M. Berg, J. L. Tymoczko, G. J. Gatto and L. Stryer, *Biochemistry. Chapter: Hemoglobin*, Macmillan Education, 2015.
5. <http://www.umich.edu/~projbnb/cvr/O2transport.pdf>, Accessed June 2020.
6. Extracorporeal Life Support Organization available from <http://www.elseo.org>.
7. NOVALUNG, <https://www.xenios-ag.com/novalung/products/>.
8. TERUMO, <http://www.terumo-cvs.com/products/ProductDetail.aspx?groupId=1&familyID=1&country=1>.
9. SORIN, <http://www.livanova.sorin.com/file/view-1559.action>.
10. J. A. Potkay, *Lab on a Chip*, **2014**, *14*, 4122-4138.
11. N. Rochow, A. Manan, W. I. Wu, G. Fusch, S. Monkman, J. Leung, E. Chan, D. Nagpal, D. Predescu, J. Brash, P. R. Selvaganapathy and C. Fusch, *Artificial organs*, **2014**, *38*, 856-866.
12. W. I. Wu, N. Rochow, E. Chan, G. Fusch, A. Manan, D. Nagpal, P. R. Selvaganapathy and C. Fusch, *Lab on a Chip*, **2013**, *13*, 2641-2650.
13. G. Raffaelli, S. Ghirardello, S. Passera, F. Mosca and G. Cavallaro, *Front. Physiol.*, **2018**, *9*, 1739.
14. M. M. Chlebowski, S. Baltagi, M. Carlson, J. H. Levy and P. C. Spinella, *Critical Care*, **2020**, *24*, 19-31.
15. O. ECLS, *ELSO anticoagulation guideline. The Extracorporeal Life Support*, 2014.
16. D. M. Hoganson, J. L. Anderson, E. F. Weinberg, E. J. Swart, B. K. Orrick, J. T. Borenstein and J. P. Vacanti, *The Journal of Thoracic and cardiovascular surgery*, **2010**, *140*, 990-995.
17. T. Kniazeva, J. C. Hsiao, J. L. Charest and J. T. Borenstein, *Biomedical Microdevices*, **2011**, *13*, 315-323.
18. R. Screenivasan, E. K. Bassett, D. M. Hoganson, J. Vacanti and K. K. Gleason, *Biomaterials*, **2011**, *32*, 3883-3889.
19. N. Rochow, W. I. Wu, E. Chan, D. Nagpal, G. Fusch, P. R. Selvaganapathy, S. Monkman and C. Fusch, *Micro Electro Mechanical systems (MEMS)*, **2012**, *2012 IEEE 25th International Conference on January 29 to February 2*, 957-960.
20. A. A. Gimbel, E. Flores, A. Koo, G. Garcia-Cardena and J. Borenstein, *Lab on a Chip*, **2016**, *16*, 3227-3234.
21. J. T. Borenstein, H. Terai, K. R. King, E. J. Weinberg and M. R. Kaazempur-Mofrad, *Biomedical Microdevices*, **2002**, *4*, 167-175.
22. M. Shin, K. Matsuda, O. Ishii, H. Terai, M. Kaazempur-Mofrad, J. Borenstein, M. Detmar and J. P. Vacanti, *Biomedical Microdevices*, **2004**, *6*, 269-278.
23. T. Kniazeva, A. E. Epshteyn, J. C. Hsiao, E. S. Kim, V. B. Kolachalama, J. L. Charest and J. T. Borenstein, *Lab on a Chip*, **2012**, *12*, 1686-1695.
24. D. M. Hoganson, H. I. Pryor, E. K. Bassett, I. D. Spool and J. P. Vacanti, *Lab on a Chip*, **2010**, *11*, 700-707.
25. J. A. Potkay, M. Magnetta, A. Vinson and B. Cmolik, *Lab on a Chip*, **2011**, *11*, 2901-2909.
26. A. J. Thompson, L. J. Ma, T. J. Plegue and J. A. Potkay, *IEEE Transactions on Biomedical Engineering*, **2019**, *66*, 1082-1093.
27. A. J. Thompson, L. H. Marks, M. J. Goudie, A. Rojas-Pena, H. Handa and J. A. Potkay, *Biomicrofluidics*, **2017**, *11*, 024113.
28. H. Matharoo, M. Dabaghi, N. Rochow, G. Fusch, N. Saraei, M. Tauhiduzzaman, S. Veldhuis, J. Brash, C. Fusch and P. R. Selvaganapathy, *Biomicrofluidics*, **2018**, *12*, 014107.

29. M. Dabaghi, G. Fusch, N. Saraei, N. Rochow, J. Brash, C. Fusch and P. R. Selvaganapathy, *Biomicrofluidics*, **2018**, *12*, 044101.
30. M. Dabaghi, N. Saraei, G. Fusch, N. Rochow, J. Brash, C. Fusch and P. R. Selvaganapathy, *Lab on a Chip*, **2018**, *18*, 3780-3789.
31. M. Malankowska, I. Julian, I. Pellejero, H. S. Rho, S. Schlautmann, R. M. Tiggelaar, M. P. Pina, H. J. G. E. Gardeniers and R. Mallada, *Sensors and Actuators B: Chemical*, **2019**.
32. E. Lamperti, R. Manno, M. Urbiztondo, M. Malankowska, M.P. Pina and R. Mallada, presented in part at the Euromembrane, Valencia, Spain, 2018.
33. C. D. Murray, *Proceedings of the national academy of sciences of the united states of america*, **1926**, *12*, 207-214.
34. J. A. Potkey, *Biomedical Microdevices*, **2013**, *15*, 397-406.
35. J. Zhang, T. D. C. Nolan, T. Zhang, B. P. Griffith and Z. J. Wu, *Journal of Membrane Science*, **2007**, *288*, 268-279.
36. S. McKee, E. A. Dougall and N. J. Mottram, *Journal of Mathematics in Industry*, **2016**, *6*, 1-22.
37. I. Rea, E. Orabona, A. Lamberti, I. Rendina and L. De Stefano, *Biomicrofluidics*, **2011**, *5*, 034120-034120-034110.
38. S. Bhattacharya, A. Datta, J. M. Berg and S. Gangopadhyay, *Journal of Microelectromechanical Systems*, **2005**, *14*, 590-597.
39. J. D. Andrade, V. Hladly, A-P. Wei, C-H. Ho, A. S. Lea, S. I. Jeon, Y. S. Lin and E. Stroup, *Clinical Materials*, **1992**, *11*, 67-84.
40. L. Yeong-Shang, V. Hladly and J. Janatova, *Biomaterials*, **1992**, *13*, 497-504.
41. L. F. Mockros and K. E. Cook, *Engineering design of thoracic artificial lung. The artificial lung*, Biosciences Publishers, 2002.
42. Safe, high-performance oxygenators for the smallest patients, <https://www.getinge.com/int/product-catalog/quadrox-i-neonatal-and-pediatric/>. , Accessed December 2018.